

# Analysis of the Single Phase Thyristor Bridge Rectifier Circuit with Inductive Load Containing Counter Electromotive Force

Susumu OHYA and Takeaki MORI

## Abstract

As seen in the a.c. electric railroad, when a sinusoidal voltage is applied to the single phase rectifier circuit with inductive load containing counter electromotive force, higher harmonic components of considerable size appear in the a.c. side current waveform. These components become the cause of the reduced power factor or the electromagnetic inductive interference.

This report presents the circuit analysis with general circuit conditions for the simplified thyristor bridge rectifier circuit. In this analysis, we separated the seven operating modes in order to grasp their fundamental behavior and made clear the effect of control angle on the region of the operating modes. Also, we studied quantitatively about the influences of control angle on the a.c. side, such as the contents of the higher harmonic components and others, by means of numerical calculations.

## 1. Introduction

With the wide adoption of power semiconductor devices represented by thyristor, higher harmonics generated by such devices are becoming important problem. Particularly, in the a.c. electric railroad, the higher harmonics contained in a.c. current due to the apparatus placed in the vehicles (transformers, rectifiers, smoothing reactors and d.c. series motors) are considerable magnitude up to the higher order. It is the well known fact that the problems are arising, in which the lower order components of harmonics make lower the power factor and the higher order components cause the electromagnetic inductive interference to neighborhood communication lines.

Therefore, it is very significant to obtain the various characteristics in a.c. side current, by the analysis of the rectifier circuit with inductive loads containing counter emf (electromotive force). Concerning to this kind of problem, investigated results have been reported up to present<sup>(1)-(5)</sup>, however, in these reports only the case of continuous current with the commutation state (it corresponds to behavior mode  $\text{IV}$  in this paper) is mentioned. On the other hand, the general analysis for the four behavior modes, considering the continuous and discontinuous states of current, is reported only for the diode bridge type rectifier circuit corresponding to control angle  $\alpha=0^\circ$  of thyristor<sup>(6)</sup>.

Therefore, in this paper, a circuit analysis of the thyristor bridge type rectifier circuit with counter emf in inductive load is described for general circuit conditions. In this analysis, we investigated the various characteristics of a.c. side current, as well as the fundamental behavior. That is, we analyzed the three behavior states—interruption, rectification and commutation (Chap. 2), and then we made clear the relation between circuit conditions and the regions of each behavior modes, separating the case of domination by control angle  $\alpha$  and by natural conduction angle  $\gamma$ , for each of the four behavior

modes. And then, we showed the effect of the change of  $\alpha$  on the region of behavior modes (Chap. 3). Further from these analyzed results, for the arbitrary circuit conditions, we studied quantitatively about the influence of control angle  $\alpha$  on the several characteristics at the a.c. side, such as the contents of the high order harmonics and power factor etc., which are the problems in a.c. electric railroad (Chap. 4).

It seems that the results of this analysis are very useful to understand the fundamental behavior and the principle of such problem and to grasp the several characteristics on a.c. side. Further, in this report, the region for only  $0^\circ \leq \alpha \leq 90^\circ$  is studied, but we wish to report, in the next chance, about the region for  $\alpha > 90^\circ$  which corresponds to the power regeneration region.

## 2. Circuit Analysis of Three Behavior State

Fig. 1 shows a single phase thyristor bridge rectifier circuit with inductive load including counter emf. In this circuit, a.c. side is composed of a leakage impedance  $Z_a = R_a + jX_a$  due to the power source transformer, and d.c. side is composed of an impedance  $Z_d = R_d + jX_d$  (smoothing reactor, d.c. series motor etc.) and a constant counter emf  $E^*$ . In this circuit the behavior of thyristor can take one of the three different states according to the control angle  $\alpha$  of thyristor and the circuit conditions. These are interruption, rectification and commutation states.

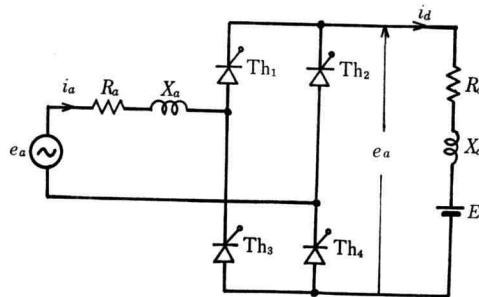


Fig. 1. Single phase thyristor bridge type rectifier circuit.

### (1) Interruption State "I" (All thyristors are at OFF state)

As Fig. 2(a) shows, when the rectification state "R", as described later, is completed with the extinction angle  $\beta$ , and if d.c. side voltage  $e_d$  is smaller than  $E$ , the current cannot flow because of the inverse voltage on thyristors. This period is named as I state, and kept until the control angle  $\alpha$ . But, if natural conduction angle  $\gamma$  ( $\gamma = \sin^{-1} E/E_m$ ) is greater than  $\alpha$ , this interruption state continues until the phase angle  $\gamma$  is reached as the manner seen in the diode type bridge. The instantaneous voltage  $e_d$  of this period is equal to  $E$ .

\* In the actual circuit, it does not cause large error even if the resistance is neglected because it is made small value in order to decrease the electrical loss<sup>(5)</sup>. We have neglected the resistance parts in halfway of this report in order to prevent the complication due to many parameters.

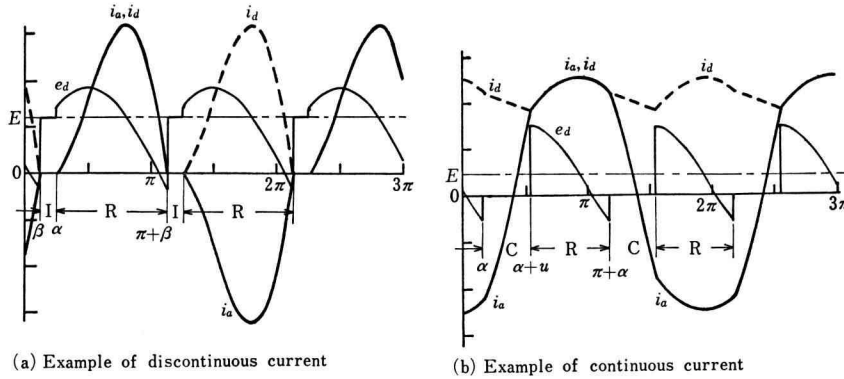


Fig. 2. Schematic illustrations of the voltage and current.

(2) Rectification State "R" ( $Th_1$  and  $Th_4$  or  $Th_2$  and  $Th_3$  are at ON state)

In the case of discontinuous current, as shown in Fig. 2(a), the rectification state R continues between control angle  $\alpha$  or  $\gamma$  of preceding paragraph and  $\pi + \beta$ . But, when there is the commutation state described in (3), as shown in Fig. 2(b), the rectification state starts when the commutation state is over. If rectification period  $\theta$  is assumed as  $\theta_R \leq \theta \leq \theta_c$ , and if  $X = X_a + X_d$ , the circuit equation is given in the following differential equation.

$$Ri_a + X \frac{di_a}{d\theta} + E = E_m \sin \theta. \quad (1)$$

The solution is

$$i_a = \frac{E_m}{Z} \{ \sin(\theta - \varphi) - \sin(\theta_R - \varphi) e^{-R/X(\theta - \theta_R)} \} + \frac{E}{R} \{ e^{-R/X(\theta - \theta_R)} - 1 \} + i_{\theta_R} e^{-R/X(\theta - \theta_R)} \quad (2)$$

where,  $Z = R + jX$ ,  $R = R_a + R_d$ ,  $X = X_a + X_d$ ,  $\varphi = \tan^{-1}(X/R)$  and  $i_{\theta_R}$  is the initial current at rectification starting angle  $\theta_R$ . When the resistances can be neglected,

$$i_a = \frac{E_m}{X} (\cos \theta_R - \cos \theta) - \frac{E}{X} (\theta - \theta_R) + i_{\theta_R} \quad (3)$$

then, d.c. voltage  $e_d$  is given as the following equation

$$e_d = X_d \frac{di_a}{d\theta} + E = E_m \frac{X_d}{X} \sin \theta + E \left( 1 - \frac{X_d}{X} \right). \quad (4)$$

## (3) Commutation State "C" (All thyristors are at ON state)

When the control signals are applied on the thyristors which are so far at OFF state before the end of rectification state, and if the natural commutation conditions are satisfied,

these thyristors are turned on. When natural commutation angle is taken as  $\gamma_m$  as described later, and if  $\gamma_m \geq \alpha$ , then commutation state starts at  $\gamma_m$ . If  $\gamma_m < \alpha$ , then commutation state is  $\alpha \leq \theta \leq \alpha + u$  as shown in Fig. 2(b), where  $u$  is the overlapping angle. Generally, when commutation state is expressed by  $\theta_c \leq \theta \leq \theta_c + u$ , equations of this circuit are

$$R_a i_a + X_a \frac{di_a}{d\theta} = E_m \sin(\theta + \theta_c), \quad (5)$$

$$R_d i_d + X_d \frac{di_d}{d\theta} + E = 0. \quad (6)$$

Taking  $i_{\theta_c}$  as the initial current at  $\theta = \theta_c$  and  $\varphi_a = \tan^{-1}(X_a/R_a)$ , the solutions are

$$i_a = \frac{E_m}{Z_a} \{ \sin(\theta - \varphi_a) - \sin(\theta_c - \varphi_a) e^{-R_a/X_a(\theta - \theta_c)} \} - i_{\theta_c} e^{-R_a/X_a(\theta - \theta_c)}, \quad (7)$$

$$i_d = i_{\theta_c} e^{-R_d/X_d(\theta - \theta_c)} + \frac{E}{R_d} \{ e^{-R_d/X_d(\theta - \theta_c)} - 1 \}. \quad (8)$$

If the resistances  $R_a$ ,  $R_d$  can be neglected, equations (7) and (8) are transformed to the following equations:

$$i_a = \frac{E_m}{X_a} (\cos \theta_c - \cos \theta) - i_{\theta_c}, \quad (9)$$

$$i_d = i_{\theta_c} - \frac{E}{X_d} (\theta - \theta_c). \quad (10)$$

As  $i_a$  is equal to  $i_d$  at the end of commutation state, i.e. at  $\theta = \theta_c + u$ , from eq. (9), (10), equation (11) is obtained.

$$i_{\theta_c} = \frac{1}{2} \left[ \frac{E_m}{X_a} \{ \cos \theta_c - \cos(\theta_c + u) \} + \frac{E}{X_d} u \right]. \quad (11)$$

The current at the end of commutation period

$$i_{\theta_c + u} = i_{\theta_c} - \frac{E}{X_d} u. \quad (12)$$

In the case of continuous current, this current  $i_{\theta_c + u}$  is the initial rectification current  $i_{\theta_R}$ . And the d.c. voltage  $e_d$  is equal to zero in this state.

Hereafter, voltage is normalized with respect to the maximum source voltage  $E_m$ , and current is normalized with respect to the current corresponding to the total reactance  $X$ . The normalized values are expressed with additional bar above each symbol, for example, such as  $\bar{E}$  or  $\bar{i}_a$ . Also, the ratio of  $X_d$  to  $X$  is expressed by  $\bar{X}_d$ .

In this manner, the above mentioned equations which are related to three states are rewritten as follows.

Interruption state:

$$\bar{i}_a = \bar{i}_d = 0$$

$$\bar{e}_d = \bar{E}$$

Rectification state:

$$\bar{i}_a = \bar{i}_d = \cos \theta_R - \cos \theta - \bar{E}(\theta - \theta_R) + \bar{i}_{\theta_R} \quad (13)$$

$$\bar{e}_d = \bar{X}_d \sin \theta + \bar{E}(1 - \bar{X}_d) \quad (14)$$

Commutation state:

$$\bar{i}_a = \frac{1}{1 - \bar{X}_d} (\cos \theta_c - \cos \theta) - \bar{i}_{\theta_c} \quad (15)$$

$$\bar{i}_d = \bar{i}_{\theta_c} - \frac{\bar{E}}{\bar{X}_d} (\theta - \theta_c) \quad (16)$$

$$\bar{e}_d = 0$$

At the start of Commutation state:

$$\bar{i}_{\theta_c} = \frac{1}{2} \left[ \frac{1}{1 - \bar{X}_d} \{ \cos \theta_c - \cos (\theta_c + u) \} + \frac{\bar{E}}{\bar{X}_d} u \right] \quad (17)$$

At the end of commutation state:

$$\bar{i}_{\theta_c + u} = \bar{i}_{\theta_c} - \frac{\bar{E}}{\bar{X}_d} u \quad (18)$$

### 3. Four Modes of Operation and their Regions

#### 3.1 Each mode of operation and waveforms of voltage and current

Mode of operation can be expressed by the combination of "I", "R" and "C" states as

Table 1 The states and their period at each operation mode.

Mode	State of behavior	Operating period
I <sub>α</sub> I <sub>γ</sub>	I · R	β <sub>1</sub> — α — π + β <sub>1</sub> β <sub>1</sub> — γ — π + β <sub>1</sub>
II	R	β <sub>2</sub> — π + β <sub>2</sub>
III <sub>α</sub> III <sub>γ</sub>	C · R · I · R	α — α + u <sub>3</sub> — β <sub>3</sub> — γ — π + α γ <sub>3</sub> — γ <sub>3</sub> + u <sub>3</sub> — β <sub>3</sub> — γ — π + γ <sub>3</sub>
IV <sub>α</sub> IV <sub>γ</sub>	C · R	α — α + u <sub>4</sub> — π + α γ <sub>4</sub> — γ <sub>4</sub> + u <sub>4</sub> — π + γ <sub>4</sub>

I: Interruption  
C: Commutation

R: Rectification

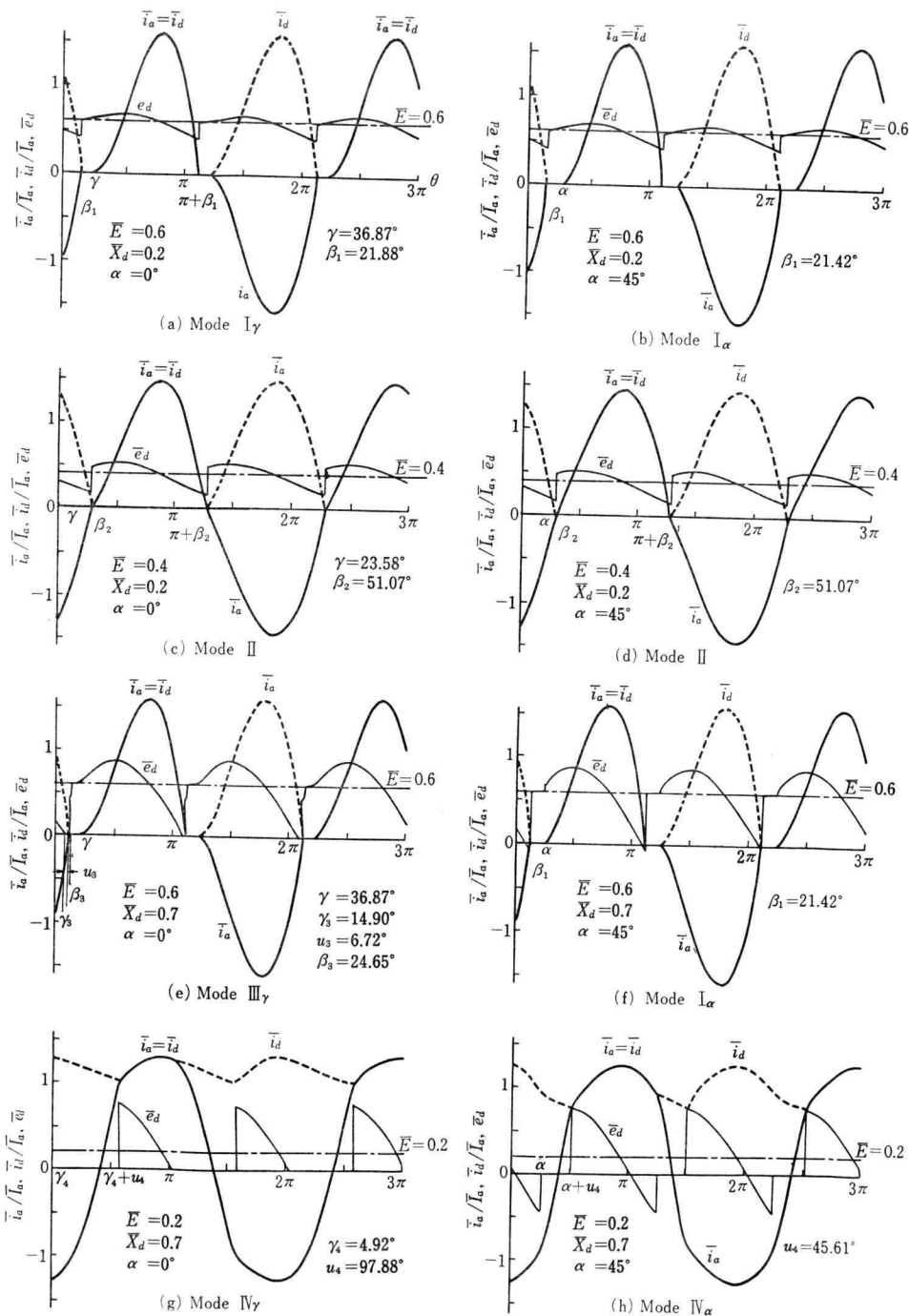


Fig. 3. Typical example of the voltage and current waveforms in each modes.

mentioned above. The diode bridge ( $\alpha=0^\circ$ ) have four modes. In the case of thyristor bridge, mode numbers are fundamentally four, as same as the diode bridge (I, II, III, IV). But, in practice, seven modes can be considered as shown in Table 1. Subscript  $\alpha$  is taken when rectification or commutation starts at control angle  $\alpha$ , and subscript  $\gamma$  is taken in other case.

Fig. 3 shows typical examples of voltage and current waveforms of each modes. In here,  $\bar{E}$  and  $\bar{X}_d$  are taken as the parameters. The figures on the left row are the cases of  $\alpha=0^\circ$  and those on the right row are the cases of  $\alpha=45^\circ$ . The subscript numbers on  $\beta$ ,  $\gamma$  and  $u$  show the assignment to each mode.

#### (1) Mode I <sub>$\alpha$</sub> and I <sub>$\gamma$</sub>

As shown in Fig. 2(a), if the behavior is I state at  $\beta \leq \theta \leq \alpha$ , and is R state at  $\alpha \leq \theta \leq \pi + \beta$ , and assuming  $\theta_R = \alpha$ , and  $i_{\theta R} = 0$  in equation (13), the a.c. current takes the form as

$$\bar{i}_a = \cos \alpha - \cos \theta - \bar{E}(\theta - \alpha). \quad (19)$$

Because this a.c. current  $\bar{i}_a$  is zero at  $\theta = \pi + \beta_1$ ,

$$\cos \alpha + \cos \beta_1 - \bar{E}(\pi + \beta_1 - \alpha) = 0. \quad (20)$$

If natural conducting angle  $\gamma$  is greater than  $\alpha$ , the mode becomes under control of  $\gamma$  (mode I <sub>$\gamma$</sub> ), and replacing  $\alpha$  by  $\gamma$  in equations (19), (20), equation (21) is obtained.

$$\left. \begin{aligned} \bar{i}_a &= \cos \gamma - \cos \theta - \bar{E}(\theta - \gamma), \\ \cos \gamma + \cos \beta_1 - \bar{E}(\pi + \beta_1 - \gamma) &= 0. \end{aligned} \right\} \quad (21)$$

In the equations (20), (21),  $\beta_1$  was calculated by Newton-Raphson method.

Effective value  $\bar{I}_a$  of a.c. current in mode I <sub>$\alpha$</sub>  can be calculated using  $\bar{i}_a$  in the equation (19) as follows, (cf. Appendix 1)

$$\bar{I}_a = \sqrt{\frac{1}{\pi} \int_{\alpha}^{\pi + \beta_1} \bar{i}_a^2 d\theta}. \quad (22)$$

Current waveforms of Fig. 3 are shown by using the ratio of  $\bar{i}_a$  to  $\bar{I}_a$  (that is  $\bar{i}_a/\bar{I}_a$ ). Fig. 3(a) shows the case of  $\bar{E}=0.6$  and  $\alpha=0^\circ$ , and then the rectification state starts at  $\gamma = \sin^{-1} \bar{E} = 36.87^\circ$ . On the other hand, Fig. 3(b) shows when the rectification starts at  $\theta = 45^\circ$  because of  $\alpha < \gamma$ .

#### (2) Mode II

In mode II, all period is R state. Putting  $\theta_R = \beta_2$  in equation (13)

$$\bar{i}_a = \cos \beta_2 - \cos \theta - \bar{E}(\theta - \beta_2) + \bar{i}_{\beta_2} \quad (23)$$

where  $\bar{i}_{\beta_2} = 0$  and because  $\bar{i}_a = 0$  at  $\theta = \pi + \beta_2$ ,  $\beta_2$  can be determined in the following equation

$$\cos \beta_2 = \frac{\pi}{2} \bar{E}. \quad (24)$$

Fig. 3(c) shows the waveforms of voltage and current for  $\bar{E}=0.4$ . In mode  $\mathbb{I}$ , both waveforms at  $\alpha=0^\circ$  and  $\alpha=45^\circ$  are identical, because  $\beta_2$  in this mode is determined only by  $\bar{E}$ .

Here, the current waveform is expressed by  $\bar{i}_a/\bar{I}_a$ , taking  $\bar{I}_a$  as  $\bar{I}_a = \sqrt{\frac{1}{\pi} \int_{\beta_2}^{\pi+\beta_2} \{eq. (23)\}^2 d\theta}$ , and voltage waveform is expressed equation (14).

### (3) Mode $\mathbb{I}_\gamma$ and $\mathbb{I}_\alpha$

Waveform in mode  $\mathbb{I}_\gamma$ , when  $\bar{E}=0.6$ ,  $\bar{X}_d=0.7$  and  $\alpha=0^\circ$ , is shown in Fig. 3(e). Before the end of rectification  $\bar{e}_d$  becomes zero and the commutation starts instantly because the remaining arms become conductive. This commutation starting angle  $\theta_c$  is named as  $\gamma_3$  and from equation (14)

$$\gamma_3 = \sin^{-1} \left[ \left( \frac{1}{\bar{X}_d} - 1 \right) \bar{E} \right]. \quad (25)$$

In the state of rectification,  $\gamma \leq \theta \leq \pi + \gamma_3$ , and taking into account that  $\bar{i}_a = \bar{i}_{\gamma_3}$  at  $\theta = \pi + \gamma_3$ ;

$$\bar{i}_{\gamma_3} = \cos \gamma - \cos (\pi + \gamma_3) - \bar{E} (\pi + \gamma_3 - \gamma). \quad (26)$$

Also, from equation (17),

$$\frac{1}{1 - \bar{X}_d} \{ \cos \gamma_3 - \cos (\gamma_3 + u_3) \} + \frac{\bar{E}}{\bar{X}_d} u_3 - 2 \bar{i}_{\gamma_3} = 0. \quad (27)$$

If  $\bar{E}$  and  $\bar{X}_d$  are given,  $\gamma_3$  and  $u_3$  are obtained from equation (25)~(27).

At the rectification state after the commutation,  $\theta$  is  $\gamma_3 + u_3 \leq \theta \leq \beta_3$ , and the starting current of rectification is shown by

$$\bar{i}_{\gamma_3+u_3} = \bar{i}_{\gamma_3} - \frac{\bar{E}}{\bar{X}_d} u_3. \quad (28)$$

Because the rectification current  $\bar{i}_a = 0$  at  $\theta = \beta_3$ , following equation is obtained from equation (13)

$$\cos (\gamma_3 + u_3) - \cos \beta_3 - \bar{E} (\beta_3 - \gamma_3 - u_3) + \bar{i}_{\gamma_3+u_3} = 0. \quad (29)$$

From  $u_3$  and  $\gamma_3$  obtained previously and from equations (27)~(29),  $\beta_3$  is also obtained by means of a numerical calculation. This mode exists when  $\beta_3 \leq \gamma$ . If  $\bar{E}=0.6$ ,  $\bar{X}_d=0.7$ , then  $\gamma_3=14.9^\circ$  and the example of Fig. 3(e) shows this case. For  $\alpha < \gamma_3$ , the mode is  $\mathbb{I}_\gamma$ , but for  $\alpha \geq \gamma_3$ , it becomes mode  $\mathbb{I}_\alpha$  by forced commutation and this mode  $\mathbb{I}_\alpha$  continues until  $\alpha = \beta_1$ . If  $\alpha = 45^\circ$ , the mode becomes  $\mathbb{I}_\alpha$  because  $\alpha \geq \beta_1$ .

### (4) Mode $\mathbb{I}$

In this mode, always the current is conducting and the overlapping angle is  $u_4$ . The



commutating current with control angle  $\alpha$  is indicated as follows,

$$\bar{i}_a = \frac{1}{1-\bar{X}_d} (\cos \alpha - \cos \theta) - \bar{i}_\alpha, \quad (30)$$

$$\bar{i}_d = \bar{i}_\alpha - \frac{\bar{E}}{\bar{X}_d} (\theta - \alpha), \quad (31)$$

and the starting current of commutation  $\bar{i}_\alpha$  in the above equations is obtained from equation (17) as follows

$$\bar{i}_\alpha = \frac{1}{2} \left[ \frac{1}{1-\bar{X}_d} \{ \cos \alpha - \cos (\alpha + u_d) \} + \frac{\bar{E}}{\bar{X}_d} u_d \right]. \quad (32)$$

Since the rectification state of this mode begins at the end of commutation,  $\theta = \alpha + u_d$ , the starting current of rectification  $\bar{i}_{\alpha+u_d}$  and the current in the rectification state  $\bar{i}_a$  can be shown as

$$\bar{i}_{\alpha+u_d} = \bar{i}_\alpha - \frac{\bar{E}}{\bar{X}_d} u_d, \quad (33)$$

$$\bar{i}_a = \cos (\alpha + u_d) - \cos \theta - \bar{E} (\theta - \alpha - u_d) + \bar{i}_\alpha - \frac{\bar{E}}{\bar{X}_d} u_d. \quad (34)$$

The overlapping angle  $u_d$  is obtained from the following equation, because  $\bar{i}_a = \bar{i}_\alpha$  at  $\theta = \pi + \alpha$ ,

$$\cos (\alpha + u_d) + \cos \alpha - \bar{E} \left( \pi - u_d + \frac{u_d}{\bar{X}_d} \right) = 0 \quad (35)$$

The instantaneous d.c. voltage  $\bar{e}_d$  is the same as given in equation (14). In the natural commutation when  $\alpha$  is smaller than  $\gamma_d$ , the starting angle of commutation  $\gamma_d$  (for  $\bar{e}_d = 0$ ) is

$$\gamma_d = \sin^{-1} \left\{ \left( \frac{1}{\bar{X}_d} - 1 \right) \bar{E} \right\}, \quad (36)$$

as same as that described for mode  $\text{III}_\gamma$ . This means that the mode  $\text{IV}_\gamma$  exists when  $\alpha \leq \gamma_d$ , and the overlapping angle and current are given by substituting  $\alpha$  by  $\gamma_d$  in equation (30)~(35).

Fig. 3(g) and (h) show the waveforms of mode  $\text{IV}$  at  $\alpha = 0^\circ$  and  $\alpha = 45^\circ$  respectively.

There is a situation in which the d.c. current are perfectly smoothed in the mode  $\text{IV}$ . For example, at  $\bar{E} = 0$  and  $\alpha = 0^\circ$ , a.c. current is sinusoidal and the harmonics are not generated. When  $\alpha = 0^\circ$  and  $\bar{X}_d \neq 1$ , d.c. current  $\bar{i}_d$  is almost smoothed for large  $\bar{X}_d$ , but a.c. side current becomes gradually the square wave with the increase of  $\bar{E}$ . In Fig. 4 (a), examples of voltage and current waveform are shown for this case. But, when  $\bar{E}$  increases moreover, mode becomes  $\text{III}_\gamma$  due to the interruption of current.

When the phase control (for example at  $\alpha = 45^\circ$ ) is adopted, the d.c. current is smooth, and the a.c. side current is trapezoidal for  $\bar{E} = 0$  and  $\bar{X}_d = 1$ . However for  $\bar{X}_d \neq 1$ ,

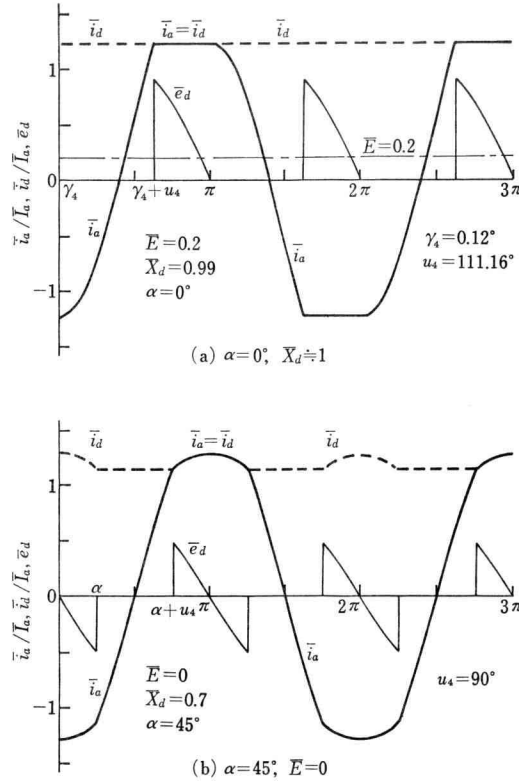


Fig. 4. Voltage and current waveforms in the exceptional case at mode II.

as is shown in Fig. 4(b), the pulsation appears in d.c. current. When  $X_d = 1$  and  $\bar{E}$  is increased, the overlapping angle decrease and the waveform of a.c. current becomes the square wave. But this mode II becomes close to the mode I<sub>a</sub> for  $u_4 \neq 0$ , and the d.c. current becomes rapidly similar to that in mode II.

### 3.2 Region of each Operational Mode

In Fig. 5, the boundaries of the regions of seven operational modes are shown. The region of Fig. 5(a) at  $\alpha = 0^\circ$  corresponds to the region of diode type bridge.

#### (1) Boundary between mode I and mode II

In the mode I<sub>a</sub> for  $\bar{X}_d \leq 0.5$ , the operation becomes mode II when extinction angle  $\beta_1$  is greater than  $\gamma$ . Replacing  $\beta_1$  and  $\alpha$  by  $\gamma$  in equation (20), and considering that  $\bar{E} = \sin \gamma$ , following equation is given:

$$2 \cos \gamma - \pi \sin \gamma = 0.$$

Then

$$\therefore \gamma = \tan^{-1} \frac{2}{\pi} = 32.48^\circ. \quad (37)$$

Hence the boundary is the line of  $\bar{E} = 0.537$ . When  $\alpha$  becomes greater than  $\gamma$  because the

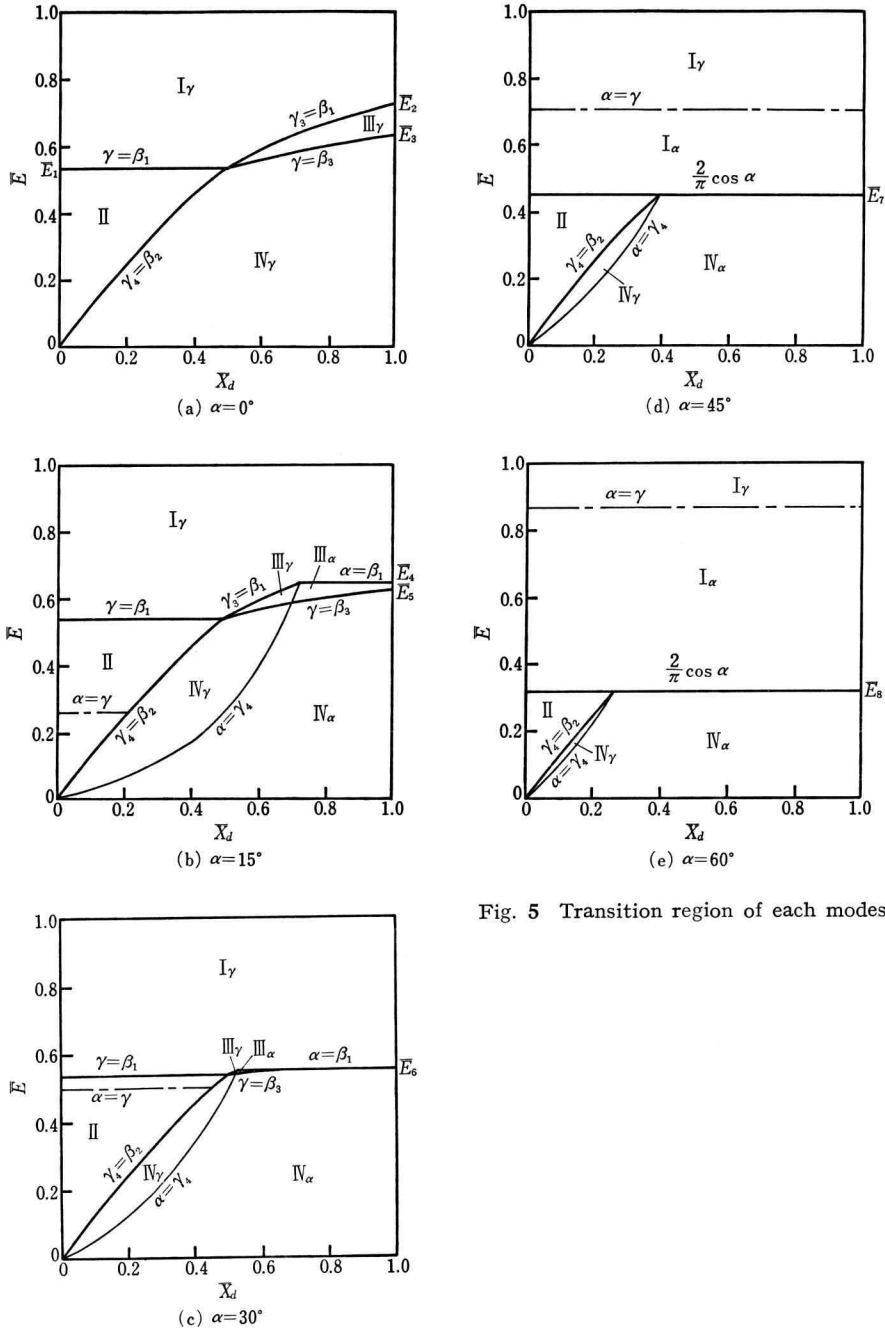


Fig. 5 Transition region of each modes.

boundary between mode I and II is the line of  $\alpha = \beta_1$ , the boundary between I and II is  $\bar{E} = 2 \cos \alpha / \pi$ , and the boundary between  $I_a$  and  $I_\gamma$  is  $\bar{E} = \sin \alpha$  when  $\bar{E} \geq 0.537$ .

(2) Boundary between mode II and mode IV

This boundary is determined by making  $\gamma_4 = \beta_2$  in equations (24) and (36) independent of  $\alpha$ , as follows

$$\sin \gamma_4 = \left( \frac{1}{\bar{X}_d} - 1 \right) \bar{E} = \sin \beta_2 = \sqrt{1 - \left( \frac{\pi}{2} \bar{E} \right)^2} . \quad (38)$$

Then

$$\bar{E} = \frac{1}{\sqrt{\left( \frac{\pi}{2} \right)^2 + \left( \frac{1}{\bar{X}_d} - 1 \right)^2}} \quad (39)$$

where  $\bar{X}_d \leq 0.5$ .

(3) Boundary between mode I and mode III

The mode III appears when  $\bar{X}_d \geq 0.5$ . The boundary of two modes is  $\gamma_3 = \beta_1$  when  $\alpha < \gamma_3$ , and  $\alpha$  is equal to  $\beta_1$  when  $\alpha \geq \gamma_3$ . These boundaries are the cases in which the relative equations as following are satisfied. For the former boundary, by making  $\sin \gamma_3 = \sin \beta_1$  following equation must be satisfied at boundary,

$$\bar{X}_d = \frac{\sin \gamma}{\sin \beta_1 + \sin \gamma} . \quad (40)$$

For the latter, from equation (21), next equation holds at boundary,

$$\cos \gamma + \cos \alpha - \bar{E} (\pi + \alpha - \gamma) = 0 . \quad (41)$$

(4) Boundary between mode III and mode IV

In the waveform of mode III, shown in Fig. 3(e), mode III transforms to mode IV, when  $\beta_3$  increases and becomes equal to  $\gamma$  and the interruption period disappears. Since this boundary can not be obtained analytically, it is given by the condition of  $\beta_3 = \gamma$  in equation (29). If  $\alpha \geq \gamma_3$ ,  $u_3$  and  $\beta_3$  are obtained from the following relations,

$$\bar{i}_\alpha = \cos \gamma - \cos (\pi + \alpha) - \bar{E} (\pi + \alpha - \gamma) , \quad (42)$$

$$\frac{\cos \alpha - \cos (\alpha + u_3)}{1 - \bar{X}_d} + \frac{\bar{E}}{\bar{X}_d} u_3 - 2 \bar{i}_\alpha = 0 , \quad (43)$$

$$\cos (\alpha + u_3) - \cos \beta_3 - \bar{E} (\beta_3 - \alpha - u_3) + \bar{i}_\alpha - \frac{\bar{E}}{\bar{X}_d} u_3 = 0 . \quad (44)$$

When the behavior is dominated by  $\alpha$ , the boundary is obtained from the condition of  $\gamma = \beta_3$ . This mode III<sub>a</sub> becomes  $I_a$  when  $\alpha = 32.48^\circ$ .

(5) Boundary between mode I and mode  $\mathbb{V}$ 

As mentioned above, mode  $\mathbb{III}$  disappears at  $\alpha \geq 32.48^\circ$ , and then the boundary between mode I and mode  $\mathbb{V}$  appears. This boundary can be expressed by  $\bar{E} = 2 \cos \alpha / \pi$ .

## 3.3 Transition between each Modes

The boundary lines shift with the value of  $\alpha$ . The value  $\bar{E}$  that is the boundary between mode I and  $\mathbb{II}$ , in Fig. 5(a), is obtained from equation (37) by making  $\bar{E}_1 = 0.537$  ( $\gamma = 32.48^\circ$ ). This boundary continues until  $\alpha = \gamma$ . The value of  $\bar{E}_2$ , that is the boundary between mode I and mode  $\mathbb{II}$  in Fig. 5(a), is nearly  $0.725$  ( $\gamma = 46.44^\circ$ ) by making  $\beta_1 = 0^\circ$  in equation (21). The boundary  $\bar{E}_3$  between mode  $\mathbb{III}$  and mode  $\mathbb{V}$  becomes  $\bar{E}_3 = 0.636$  by numerical calculation.

With the increase of the control angle  $\alpha$ , the region of the modes which is dominated by  $\alpha$  increases.

In the figure of the region for  $\alpha = 15^\circ$  shown in Fig. 5(b), new boundary lines between  $\mathbb{III}_\gamma$  and  $\mathbb{III}_\alpha$ ,  $\mathbb{V}_\gamma$  and  $\mathbb{V}_\alpha$  as well as  $\mathbb{I}_\gamma$  and  $\mathbb{III}_\alpha$  are indicated. The former two boundaries are related to the following equation:

$$\bar{E} = \frac{\bar{X}_d \sin \alpha}{1 - \bar{X}_d}, \quad (45)$$

and another boundary is determined from equation (41).

$\bar{E}_4$  and  $\bar{E}_5$  in Fig. 5(b) for  $\alpha = 15^\circ$  are nearly equal to 0.640 and 0.614 respectively from equations (41)~(44). The region of mode  $\mathbb{III}$  at  $\alpha = 30^\circ$  becomes very narrow as shown in Fig. 5(c), and the boundary between mode  $\mathbb{I}_\gamma$  and mode  $\mathbb{III}_\alpha$  becomes  $\bar{E}_6 = 0.552$ .  $\bar{E}_7 = 0.450$  and  $\bar{E}_8 = 0.318$  are the boundaries between  $\mathbb{I}_\alpha$  and  $\mathbb{V}_\alpha$  for  $\alpha = 45^\circ$  and  $\alpha = 60^\circ$  respectively. They are calculated by  $\bar{E} = 2 \cos \alpha / \pi$  since  $\alpha \geq \gamma$ . At  $\alpha \geq 32.48^\circ$ , the boundary between mode  $\mathbb{I}_\gamma$  and  $\mathbb{I}_\alpha$  is determined from  $\bar{E} = \sin \alpha$ .

## 4. Various Characteristics for A.C. Side

After the calculations of the extinction angle, the commutation angle and the overlapping angle etc. for the various values of  $\alpha$ ,  $\bar{E}$  and  $\bar{X}_d$  and after the decision of the modes, the waveforms and various characteristics are calculated for each mode. As typical example, the various characteristics in the case of  $\bar{E} = 0.2, 0.4$  and  $0.6$  are illustrated by diagrams (in Fig. 6~Fig. 11).

## 4.1 Overlapping Angle

The overlapping angle  $u$ , that represents the commutation period, exists in the cases of mode  $\mathbb{III}$  and mode  $\mathbb{V}$ , and is given by equations (27) and (35) by transforming the symbol in both equations. Fig. 6 shows the characteristics of overlapping angle. Linear parts which are independent of  $\alpha$  are the result of natural commutation. If the counter emf  $\bar{E}$  is zero, the overlapping angle  $u$  is equal to  $180^\circ - 2\alpha$ . Generally the larger  $\alpha$  results the smaller  $u$ . For  $\bar{E} = 0.6$  and  $\bar{X}_d = 0.6$ , overlapping angle  $u$  does not exist because mode I is independent

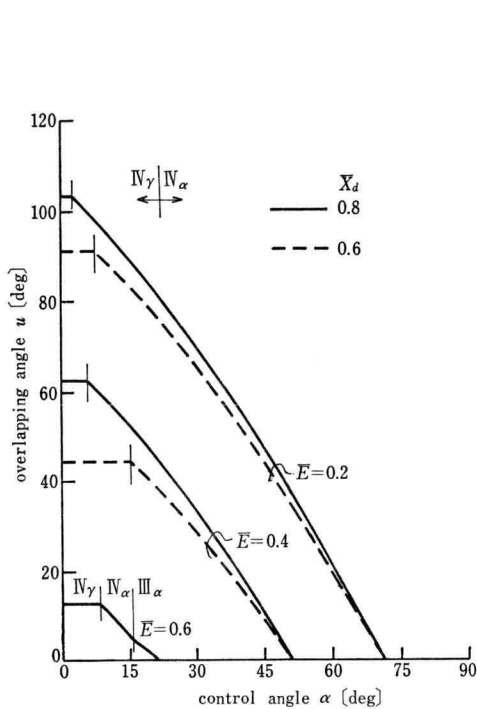


Fig. 6. Overlapping angle vs. control angle.

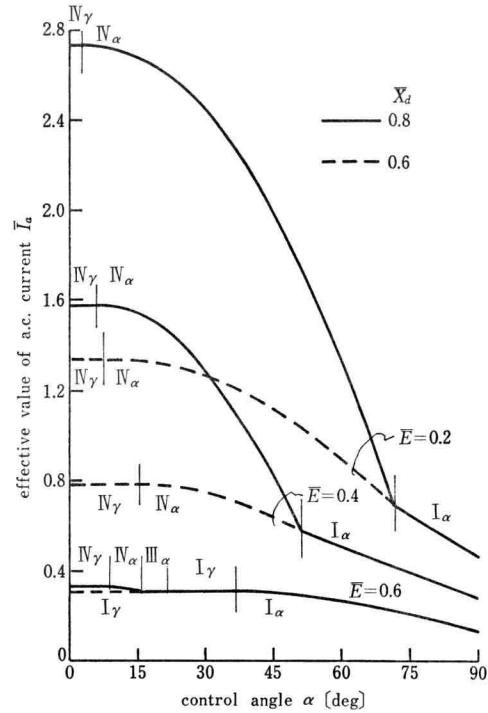


Fig. 7. Effective value of a.c. current vs. control angle.

of  $\alpha$ . For  $\bar{E}=0.6$  and  $\bar{X}_d=0.8$ , the effect of  $\alpha$  on the mode is as follows: mode  $\mathbb{N}_\gamma$  for  $\alpha \leq 8.63^\circ$ , mode  $\mathbb{N}_\alpha$  for  $8.63^\circ \leq \alpha \leq 15.9^\circ$ , mode  $\mathbb{III}_\alpha$  for  $15.9^\circ \leq \alpha \leq 21.9^\circ$  and interruption mode  $\mathbb{I}$  for  $\alpha \geq 21.9^\circ$ .

When  $\alpha \geq 32.48^\circ$ ,  $u$  becomes zero at  $\alpha = 51.07^\circ$  for  $\bar{E}=0.4$ , and  $\alpha = 71.69^\circ$  for  $\bar{E}=0.2$  from the relation  $\alpha = \cos^{-1}(\pi \bar{E}/2)$ . If  $\alpha$  is greater than these values, the mode becomes mode  $\mathbb{I}$ . When  $\alpha \leq 32.48^\circ$ ,  $u$  becomes zero on the part of the boundary of mode  $\mathbb{III}$  for  $\alpha = \beta_1$  or  $\gamma_3 = \beta_1$ , or on the boundary between mode  $\mathbb{II}$  and mode  $\mathbb{N}$  where  $\gamma_4 = \beta_2$ .

#### 4.2 Effective Value of A.C. Side Current

Since effective value of a.c. current for each modes is

$$\bar{I}_a = \sqrt{\frac{1}{\pi} \sqrt{\int_{\theta_1}^{\theta_2} \bar{i}_a^2 d\theta + \dots + \int_{\theta_1}^{\pi+\theta_1} \bar{i}_a^2 d\theta}}, \quad (46)$$

$\bar{I}_a$  may be calculated by determining the integral duration of each waveform (cf. Appendix 1). Fig. 7 shows the calculated example of effective value  $\bar{I}_a$  relative to  $\alpha$ .  $\bar{I}_a$  decreases with the increase of  $\alpha$ , and if  $\alpha$  is constant,  $\bar{I}_a$  increases with the decrease of  $\bar{E}$  or when  $\bar{X}_d$  becomes nearly 1.0.

### 4.3 Contents of Fundamental Wave and Higher Harmonics Wave

The effective value of  $n$  th harmonic component in a.c. side current is

$$\bar{I}_{an} = \frac{\sqrt{\bar{a}_n^2 + \bar{b}_n^2}}{\sqrt{2}}, \quad (47)$$

where  $\bar{a}_n$  and  $\bar{b}_n$  may be calculated from Appendix 2 and  $\bar{I}_a = \sqrt{\bar{I}_{a1}^2 + \sum_{m=1} \bar{I}_{a(2m+1)}^2}$ .

Fig. 8 shows the content of fundamental wave  $\bar{I}_{a1}/\bar{I}_a$ , and Fig. 9 shows the content of of from 3rd to 9th order harmonics. In both figures, for  $\bar{E}=0.2$  and  $0.4$ , the mode changes from  $\mathbb{V}_\gamma$  to  $\mathbb{V}_\alpha$ , and then to  $\mathbb{I}_\alpha$  with the increase of  $\alpha$ . For  $\bar{E}=0.6$ , the mode changes from  $\mathbb{I}_\gamma$  to  $\mathbb{I}_\alpha$  at  $\alpha=36.87^\circ$  when  $\bar{X}_d=0.6$ . If  $\bar{X}_d=0.8$ , then the mode changes in the order  $\mathbb{V}_\gamma$ - $\mathbb{V}_\alpha$ - $\mathbb{III}_\alpha$ - $\mathbb{I}_\gamma$  as expressed in section 4.1, and the mode changes to  $\mathbb{I}_\alpha$  above  $36.87^\circ$ .

As is evident from Fig. 9, components of higher harmonics decrease on the boundary of mode  $\mathbb{V}$  where the continuous current in mode  $\mathbb{V}$  changes to the discontinued current. In the region of discontinuous current, these components increase rapidly.

Relationship between the higher harmonics contents and the reactance ratio  $\bar{X}_d$  is shown

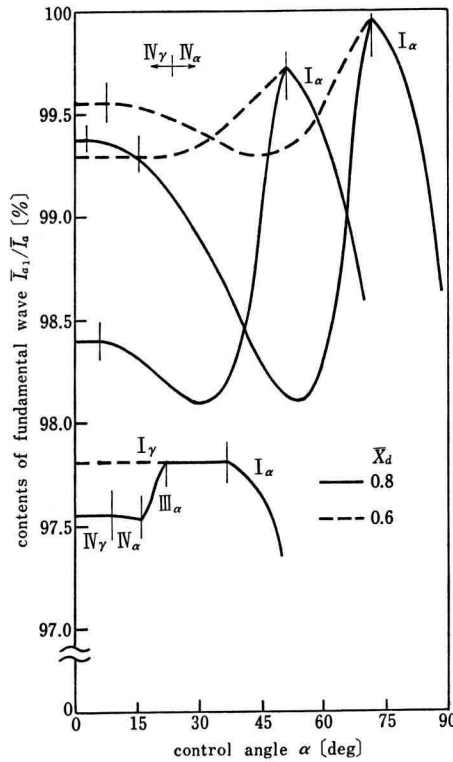


Fig. 8. Contents of fundamental wave for various  $\alpha$ .

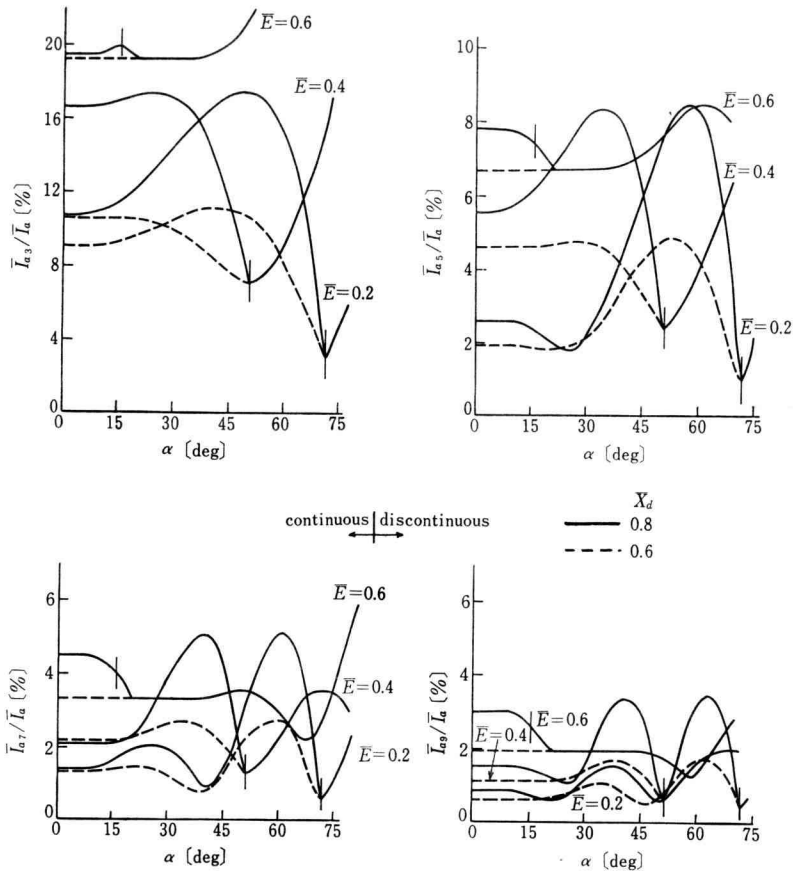


Fig. 9. Contents of 3rd~9th order harmonics vs. control angle.

in Fig. 10. In general, the overlapping angle increases with greater  $\bar{X}_d$ , and the contents of higher harmonics increase too. But, in the case of  $\alpha=60^\circ$  for  $\bar{E}=0.6$  and  $\bar{E}=0.4$ , and in the in case of  $\alpha=30^\circ$  for  $\bar{E}=0.6$ , where both modes are mode I<sub>y</sub> with discontinuous current, the higher harmonics contents are not changed by  $\bar{X}_d$  provided that  $\alpha$  is constant. When  $\alpha=0^\circ$ , mode III exists in the range  $0.617 \leq \bar{X}_d \leq 0.766$  for  $\bar{E}_d=0.6$ .

#### 4.4 Total Power Factor $pf_t$

Total power factor is given by the following equation:

$$pf_t = \frac{\sqrt{2} \bar{I} \bar{E}}{\bar{I}_a}, \quad (48)$$

where  $\bar{I}$  is obtained from the following equation since  $\bar{I}$  is the average value of d.c. current  $i_d$ :



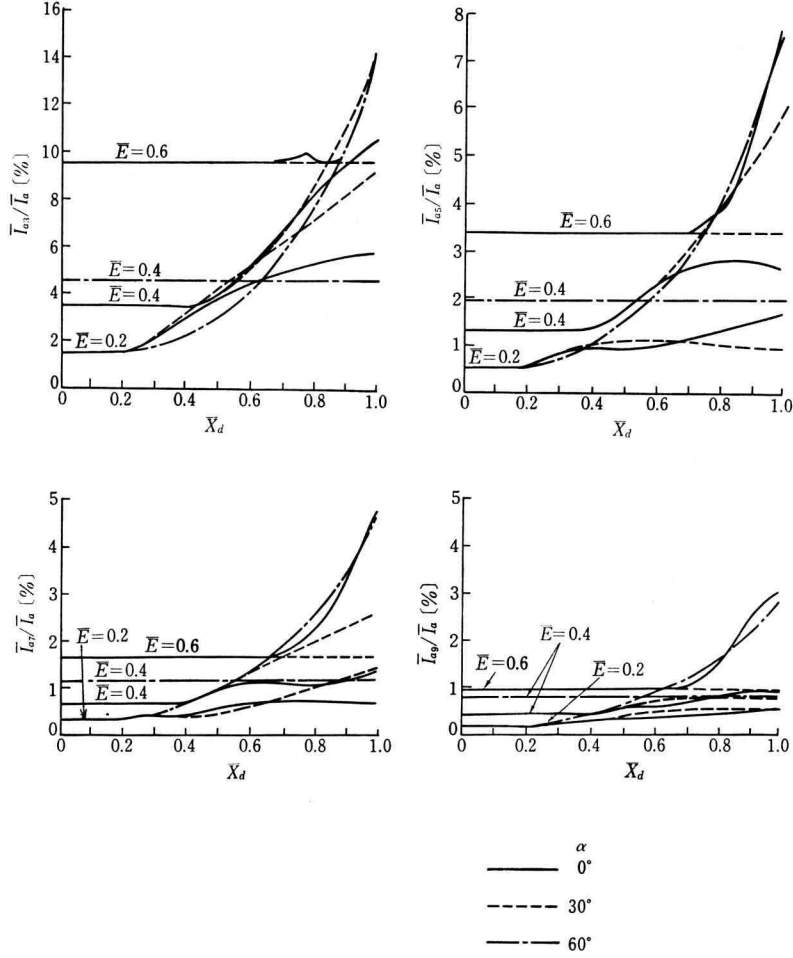


Fig. 10. Relationships between higher harmonics contents and reactance ratio  $\bar{X}_d$ .

$$\bar{I} = \sqrt{\frac{1}{\pi} \sqrt{\int_{\theta_1}^{\theta_2} \bar{i}_a d\theta + \dots + \int_{\theta_1}^{\pi+\theta_1} \bar{i}_a d\theta}} \quad (49)$$

Fig. 11 shows the relationship between total power factor  $\bar{p}f_t$  and control angle  $\alpha$ . Power factor reduces slowly with the increase of  $\alpha$ .

#### 4.5 Phase Angle of Harmonics

The phases angle  $\phi_n$  of fundamental and higher harmonics is calculated as follows,

$$\phi_n = \tan^{-1} \left( \frac{\bar{a}_n}{\bar{b}_n} \right). \quad (50)$$

Fig. 12 shows the relation between phase and  $\bar{X}_d$  with parameter  $\alpha$  in the case of  $\bar{E}=0.2$ .

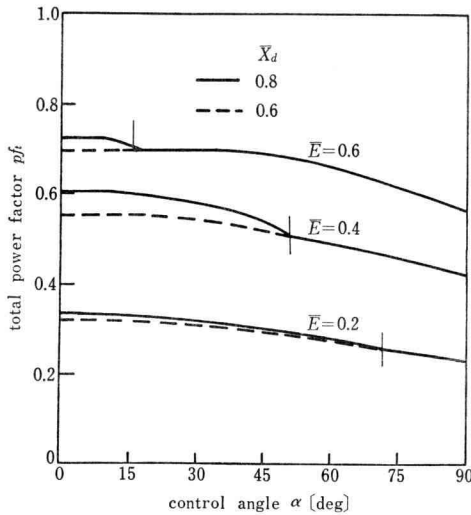


Fig. 11. Relationship between total power factor and control angle  $\alpha$ .

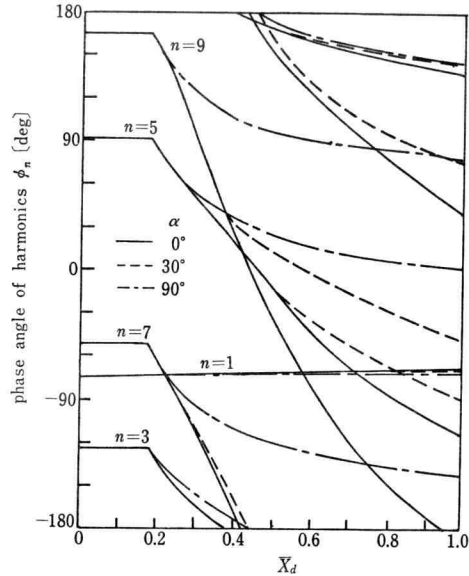


Fig. 12. Relationship between phase angle of harmonics  $\phi_n$  and reactance ratio  $\bar{X}_d$  at  $\bar{E}=0.2$ .

If  $\bar{X}_d \leq 0.18$ , the power factor is not influenced by  $\bar{X}_d$  and  $\alpha$  because the mode is II, and except for  $\alpha=60^\circ$ , the change of phase angle is large in higher order harmonics.

## 5. Conclusions

We have made analysis on the operation of the single phase thyristor bridge rectifier circuit with inductive load containing counter emf and we gave the operation modes and the various characteristics by means of the numerical calculation using the control angle  $\alpha$  and the circuit constants. The summary of results is as follows:

(1) It has become clear that the operation modes can be divided into seven classifications. There are 4 modes due to natural conduction or natural commutation as in the case of diode bridge and 3 modes dominated by control angle  $\alpha$ .

(2) The variations of the region of operation modes are shown in Fig. 5, where the boundaries are made clear.

Assuming the counter emf is constant, following three comments can be mentioned:

(3) The contents of higher harmonics for a.c. side current is the lowest on the boundary between the continuous mode  $\text{IV}_\alpha$  and the discontinuous mode  $\text{I}_\alpha$ .

(4) Generally, larger ratio of smoothing reactance  $\bar{X}_d$  results in the more contents of higher harmonics.

(5) Power factor falls gradually with increasing  $\alpha$ .

Further, as the next step, we intend to examine about the operation characteristics of the power regenerative region for  $\alpha \geq 90^\circ$  and of the hybrid bridge rectifier circuit used commonly in the electric railroad.

At the end, the authors would like to acknowledge the continuing guidance and encouragement by Prof. N. Kitashima.

### References

- 1) T. Hongo: On the Higher Harmonic Current on AC Side of the Single Phase Full-Wave Rectifier Circuit. Jour. IEE of Japan 78, 62 (1958-1)
- 2) T. Hongo: On the Higher Harmonic Currents on AC Side of the Single Phase Full-Wave Rectifier Circuit with the AC Filter (In No-Grid Control). Jour. IEE of Japan 79, 722 (1959-6)
- 3) T. Hongo: On the Higher Harmonic Currents on the AC Side of the Single Phase Full-Wave Rectifier Circuit with the AC Filter (In Grid Control). Jour. IEE of Japan 80, 35 (1960-1)
- 4) N. Irie, T. Kawazoe and T. Kawamura: Characteristic Calculation of Single Phase Rectifier Circuit Used in Electric Railway. *ibid* 87, 539 (1967-3)
- 5) N. Irie and Y. Yamazaki: Normalized Characteristics of Single Phase Rectifier Circuit used in Electric Railway. *ibid* 87, 2232 (1967-11)
- 6) T. Kawamura and S. Sone: Analysis of Fundamental Monophase Rectifier Circuit. *ibid.* 99-B62, 509 (1979-8)

### Appendix

#### 1. Effective value of a.c. side current $\bar{I}_a$

$$\left. \begin{aligned} k_1 &= \bar{E}\alpha + \cos \alpha, & k_1' &= \bar{E}\gamma + \cos \gamma, \\ k_2 &= \frac{\cos \alpha}{1 - \bar{X}_d} - \bar{i}_\alpha, \\ k_3 &= \cos(\alpha + u_3) + \bar{E}(\alpha + u_3) + \bar{i}_{\alpha_3} - \frac{\bar{E}}{\bar{X}_d} u_3, \\ k_4 &= \cos(\alpha + u_4) + \bar{E}(\alpha + u_4) + \bar{i}_{\alpha_4} - \frac{\bar{E}}{\bar{X}_d} u_4. \end{aligned} \right\} \quad (\text{Ap. 1})$$

#### (1) Mode $I_\alpha$

$$\bar{I}_a = \sqrt{\frac{1}{\pi} \int_\alpha^{\pi+\beta_1} \bar{i}_a^2 d\theta} = \sqrt{\frac{1}{\pi} \left[ \frac{\bar{E}^3}{3} \theta^3 - k_1 \bar{E} \theta^2 + k_1^2 \theta + \frac{\theta}{2} + \frac{\sin 2\theta}{4} \right.}^* \\ \left. - 2 \cos \alpha \sin \theta + 2\bar{E}(\theta \sin \theta + \cos \theta - \alpha \sin \alpha) \right]_\alpha^{\pi+\beta_1}} \quad (\text{Ap. 2})$$

#### (2) Mode $I_\gamma$

In equation (Ap. 2),  $\alpha$  replaces with  $\gamma$ ,  $k_1$  replaces with  $k_1'$ .

#### (3) Mode II

In equation (Ap. 2),  $\alpha$  and  $\beta_1$  replace with  $\beta_2$ .

#### (4) Mode III $_\alpha$

$$\bar{i}_{\alpha 3} = \frac{1}{2} \left[ \frac{1}{1 - \bar{X}_d} \{ \cos \alpha - \cos(\alpha + u_3) \} + \frac{\bar{E}}{\bar{X}_d} u_3 \right] \quad (\text{Ap. 3})$$

$$\begin{aligned}
\bar{I}_a = & \sqrt{\frac{1}{\pi}} \sqrt{\left[ k_2^2 \theta - \frac{2k_2}{1-\bar{X}_d} \sin \theta + \frac{1}{(1-\bar{X}_d)^2} \left( \frac{\theta}{2} + \frac{\sin 2\theta}{4} \right) \right]_{\alpha}^{\alpha+u_s}} * \\
& * \frac{\left[ \frac{\bar{E}^3}{3} \theta^3 - k_3 \bar{E} \theta^2 + k_3^2 \theta + \frac{\theta}{2} + \frac{\sin 2\theta}{4} - 2k_3 \sin \theta + 2\bar{E} (\cos \theta + \theta \sin \theta) \right]_{\alpha+u_s}^{\beta_s}}{**} \\
& ** \frac{\left[ \frac{\bar{E}^3}{3} \theta^3 - k_1' \bar{E} \theta^2 + k_1' \theta + \frac{\theta}{2} + \frac{\sin 2\theta}{4} - 2k_1' \sin \theta + 2\bar{E} (\cos \theta + \theta \sin \theta) \right]_{\gamma}^{\pi+\alpha}}{\gamma}
\end{aligned} \quad (\text{Ap. 4})$$

(5) Mode  $\mathbb{I}\alpha$

In equations (Ap. 3) and (Ap. 4),  $\alpha$  replaces with  $\gamma_3$

(6) Mode  $\mathbb{N}\alpha$

$$\begin{aligned}
\bar{i}_{\alpha_4} = & \frac{1}{2} \left[ \frac{1}{1-\bar{X}_d} \{ \cos \alpha - \cos (\alpha + u_4) \} + \frac{\bar{E}}{\bar{X}_d} u_4 \right] \quad (\text{Ap. 5}) \\
\bar{I}_a = & \sqrt{\frac{1}{\pi}} \sqrt{\left[ k_1^2 \theta - \frac{2k_1}{1-\bar{X}_d} \sin \theta + \frac{1}{(1-\bar{X}_d)^2} \left( \frac{\theta}{2} + \frac{\sin 2\theta}{4} \right) \right]_{\alpha}^{\alpha+u_4}} * \\
& * \frac{\left[ \frac{\bar{E}^2}{3} \theta^3 - k_4 \bar{E} \theta^2 + k_4^2 \theta + \frac{\theta}{2} + \frac{\sin 2\theta}{4} - 2k_4 \sin \theta + 2\bar{E} (\cos \theta + \theta \sin \theta) \right]_{\alpha+u_4}^{\pi+\alpha}}{\alpha+u_4}
\end{aligned} \quad (\text{Ap. 6})$$

(7) Mode  $\mathbb{N}\gamma$

In equations (Ap. 5) and (Ap. 6),  $\alpha$  replaces with  $\gamma_4$ .

## 2. Higher harmonics components and their contents in a.c. side current

Components of  $n$ th order harmonics and its contents are calculated in the following equations.

$$\bar{a}_n = \frac{2}{\pi} \left\{ \int_{\theta_1}^{\theta_2} \bar{i}_a \cos n\theta d\theta + \dots + \int_{\pi+\theta_1}^{\pi+\theta_2} \bar{i}_a \cos n\theta d\theta \right\} \quad (\text{Ap. 7})$$

$$\bar{b}_n = \frac{2}{\pi} \left\{ \int_{\theta_1}^{\theta_2} \bar{i}_a \sin n\theta d\theta + \dots + \int_{\pi+\theta_1}^{\pi+\theta_2} \bar{i}_a \sin n\theta d\theta \right\} \quad (\text{Ap. 8})$$

$$\bar{I}_{an} = \frac{\sqrt{\bar{a}_n^2 + \bar{b}_n^2}}{\sqrt{2}} \quad (\text{Ap. 9})$$

$$\text{Higher harmonics contents} = \bar{I}_{an} / \bar{I}_a \quad (\text{Ap. 10})$$

Following equations show the inducement of  $\bar{a}_n$ ,  $\bar{b}_n$  in the case of mode  $\mathbb{I}\alpha$ ,  $\mathbb{I}\gamma$ ,  $\mathbb{I}\gamma$ , and  $\mathbb{N}\alpha$ . The value of  $\bar{a}_n$ ,  $\bar{b}_n$  in mode  $\mathbb{I}\gamma$ ,  $\mathbb{I}\gamma$ ,  $\mathbb{I}\gamma$ , and  $\mathbb{N}\gamma$  can be obtained by replacement of symbols in much the same way as Appendix 1.

(1) Mode I<sub>α</sub>

$$\bar{a}_1 = \frac{2}{\pi} \left[ k_1 \sin \theta - \frac{\theta}{2} - \frac{\sin 2\theta}{4} - \bar{E} (\theta \sin \theta + \cos \theta) \right]_{\alpha}^{\pi+\beta_1} \quad (\text{Ap. 11})$$

$$\begin{aligned} \overline{a_{2m+1}} = \frac{2}{\pi} \left[ k_1 \frac{\sin (2m+1) \theta}{2m+1} - \frac{\sin 2(m+1) \theta}{4(m+1)} - \frac{\sin 2m\theta}{4m} \right. \\ \left. - \bar{E} \left\{ \frac{\cos (2m+1) \theta}{(2m+1)^2} + \frac{\theta \sin (2m+1) \theta}{2m+1} \right\} \right]_{\alpha}^{\pi+\beta_1} \end{aligned} \quad (\text{Ap. 12})$$

$$\bar{b}_1 = \frac{2}{\pi} \left[ -k_1 \cos \theta - \frac{\sin^2 \theta}{2} + \bar{E} (\theta \cos \theta - \sin \theta) \right]_{\alpha}^{\pi+\beta_1} \quad (\text{Ap. 13})$$

$$\begin{aligned} \overline{b_{2m+1}} = \frac{2}{\pi} \left[ -k_1 \frac{\cos (2m+1) \theta}{2m+1} + \frac{\cos 2(m+1) \theta}{4(m+1)} + \frac{\cos 2m\theta}{4m} \right. \\ \left. - \bar{E} \left\{ \frac{\sin (2m+1) \theta}{(2m+1)^2} - \frac{\theta \cos (2m+1) \theta}{2m+1} \right\} \right]_{\alpha}^{\pi+\beta_1} \end{aligned} \quad (\text{Ap. 14})$$

(2) Mode III<sub>α</sub>

$$\begin{aligned} \bar{a}_1 = \frac{2}{\pi} \left[ k_2 \sin \theta - \frac{1}{1-\bar{X}_d} \left( \frac{\theta}{2} + \frac{\sin 2\theta}{4} \right) \right]_{\alpha}^{\alpha+u_s} \\ + \frac{2}{\pi} \left[ k_3 \sin \theta - \left( \frac{\theta}{2} + \frac{\sin 2\theta}{4} \right) - \bar{E} (\cos \theta + \theta \sin \theta) \right]_{\alpha+u_s}^{\beta_s} \\ + \frac{2}{\pi} \left[ k_1' \sin \theta - \left( \frac{\theta}{2} + \frac{\sin 2\theta}{4} \right) - \bar{E} (\cos \theta + \theta \sin \theta) \right]_{\gamma}^{\pi+\alpha} \end{aligned} \quad (\text{Ap. 15})$$

$$\begin{aligned} \overline{a_{2m+1}} = \frac{2}{\pi} \left[ k_2 \frac{\sin (2m+1) \theta}{2m+1} - \frac{1}{1-\bar{X}_d} \left\{ \frac{\sin 2m\theta}{4m} + \frac{\sin 2(m+1) \theta}{4(m+1)} \right\} \right]_{\alpha}^{\alpha+u_s} \\ + \frac{2}{\pi} \left[ k_3 \frac{\sin (2m+1) \theta}{2m+1} - \frac{\sin 2m\theta}{4m} - \frac{\sin 2(m+1) \theta}{4(m+1)} \right. \\ \left. - \bar{E} \left\{ \frac{\cos (2m+1) \theta}{(2m+1)^2} - \frac{\theta \sin (2m+1) \theta}{2m+1} \right\} \right]_{\alpha+u_s}^{\beta_s} + \frac{2}{\pi} \left[ k_1' \frac{\sin (2m+1) \theta}{2m+1} \right. \\ \left. - \frac{\sin 2m\theta}{4m} - \frac{\sin 2(m+1) \theta}{4(m+1)} - \bar{E} \left\{ \frac{\cos (2m+1) \theta}{(2m+1)^2} - \frac{\theta \sin (2m+1) \theta}{2m+1} \right\} \right]_{\gamma}^{\pi+\alpha} \end{aligned} \quad (\text{Ap. 16})$$

$$\bar{b}_1 = \frac{2}{\pi} \left[ -k_2 \cos \theta - \frac{\sin^2 \theta}{2(1-\bar{X}_d)} \right]_{\alpha}^{\alpha+u_s} - \frac{2}{\pi} \left[ k_3 \cos \theta + \frac{\sin^2 \theta}{2} \right.$$

$$+ \bar{E}(\sin \theta - \theta \cos \theta) \Big]_{\alpha+u_s}^{\beta_s} - \frac{2}{\pi} \left[ k_1' \cos \theta + \frac{\sin^2 \theta}{2} + \bar{E}(\sin \theta - \theta \cos \theta) \right]_{\gamma}^{\pi+\alpha} \quad (\text{Ap. 17})$$

$$\begin{aligned} \bar{b}_{2m+1} = & \frac{2}{\pi} \left[ -k_2 \frac{\cos(2m+1)\theta}{2m+1} + \frac{1}{1-\bar{X}_d} \left\{ \frac{\cos 2m\theta}{4m} - \frac{\cos 2(m+1)\theta}{4(m+1)} \right\} \right]_{\alpha}^{\alpha+u_s} \\ & - \frac{2}{\pi} \left[ k_3 \frac{\cos(2m+1)\theta}{2m+1} - \frac{\cos 2m\theta}{4m} - \frac{\cos 2(m+1)\theta}{4(m+1)} + \bar{E} \left\{ \frac{\sin(2m+1)\theta}{(2m+1)^2} \right. \right. \\ & \left. \left. - \frac{\theta \cos(2m+1)\theta}{2m+1} \right\} \right]_{\alpha+u_s}^{\beta_s} - \frac{2}{\pi} \left[ k_1' \frac{\cos(2m+1)\theta}{2m+1} - \frac{\cos 2m\theta}{4m} \right. \\ & \left. - \frac{\cos 2(m+1)\theta}{4(m+1)} + \bar{E} \left\{ \frac{\sin(2m+1)\theta}{(2m+1)^2} - \frac{\theta \cos(2m+1)\theta}{2m+1} \right\} \right]_{\gamma}^{\pi+\alpha} \quad (\text{Ap. 18}) \end{aligned}$$

(3) Mode  $\mathbb{N}_\alpha$

$$\begin{aligned} \bar{a}_1 = & \frac{2}{\pi} \left[ k_2 \sin \theta - \frac{1}{1-\bar{X}_d} \left( \frac{\theta}{2} + \frac{\sin 2\theta}{4} \right) \right]_{\alpha}^{\alpha+u_s} \\ & + \frac{2}{\pi} \left[ k_4 \sin \theta - \left( \frac{\theta}{2} + \frac{\sin 2\theta}{4} \right) - \bar{E}(\cos \theta + \theta \sin \theta) \right]_{\alpha+u_s}^{\pi+\alpha} \quad (\text{Ap. 19}) \end{aligned}$$

$$\begin{aligned} \bar{a}_{2m+1} = & \frac{2}{\pi} \left[ k_2 \frac{\sin(2m+1)\theta}{2m+1} - \frac{1}{1-\bar{X}_d} \left\{ \frac{\sin 2m\theta}{4m} + \frac{\sin 2(m+1)\theta}{4(m+1)} \right\} \right]_{\alpha}^{\alpha+u_s} \\ & + \frac{2}{\pi} \left[ k_4 \frac{\sin(2m+1)\theta}{2m+1} - \left\{ \frac{\sin 2m\theta}{4m} + \frac{\sin 2(m+1)\theta}{4(m+1)} \right\} \right. \\ & \left. - \bar{E} \left\{ \frac{\cos(2m+1)\theta}{(2m+1)^2} - \frac{\theta \sin(2m+1)\theta}{2m+1} \right\} \right]_{\alpha+u_s}^{\pi+\alpha} \quad (\text{Ap. 20}) \end{aligned}$$

$$\begin{aligned} \bar{b}_1 = & \frac{2}{\pi} \left[ -k_2 \cos \theta - \frac{\sin^2 \theta}{2(1-\bar{X}_d)} \right]_{\alpha}^{\alpha+u_s} \\ & - \frac{2}{\pi} \left[ k_4 \cos \theta + \frac{\sin^2 \theta}{2} + \bar{E}(\sin \theta - \theta \cos \theta) \right]_{\alpha+u_s}^{\pi+\alpha} \quad (\text{Ap. 21}) \end{aligned}$$

$$\begin{aligned} \bar{b}_{2m+1} = & \frac{2}{\pi} \left[ -k_2 \frac{\cos(2m+1)\theta}{2m+1} + \frac{1}{1-\bar{X}_d} \left\{ \frac{\cos 2m\theta}{4m} + \frac{\cos 2(m+1)\theta}{4(m+1)} \right\} \right]_{\alpha}^{\alpha+u_s} \\ & - \frac{2}{\pi} \left[ k_4 \frac{\cos(2m+1)\theta}{2m+1} - \frac{\cos 2m\theta}{4m} - \frac{\cos 2(m+1)\theta}{4(m+1)} \right. \\ & \left. + \bar{E} \left\{ \frac{\sin(2m+1)\theta}{(2m+1)^2} - \frac{\theta \cos(2m+1)\theta}{2m+1} \right\} \right]_{\alpha+u_s}^{\pi+\alpha} \quad (\text{Ap. 22}) \end{aligned}$$